ACS Catalysis

Research Article

pubs.acs.org/acscatalysis

Mechanistic Study on Ligand-Controlled Rh(I)-Catalyzed Coupling Reaction of Alkene-Benzocyclobutenone

Qianqian Lu,[†] Bing Wang,[†] Haizhu Yu,*[,‡] and Yao Fu*[,†]

[†]Collaborative Innovation Center of Chemistry for Energy Materials, CAS Key Laboratory of Urban Pollutant Conversion, Department of Chemistry, University of Science and Technology of China, Hefei 230026, China

[‡]Department of Chemistry and Center for Atomic Engineering of Advanced Materials, Anhui University, Hefei 230601, China

Supporting Information

ABSTRACT: Recently, Dong's group [*Angew. Chem., Int. Ed.* **2012**, *51*, 7567−7571; *Angew. Chem., Int. Ed.* **2014**, *53*, 1891−1895] reported the ligand-controlled selectivity of Rh-catalyzed intramolecular coupling reaction of alkene-benzocyclobutenone: the direct coupling product (i.e., fused-rings) was formed in the DPPB-assisted system (DPPB = $PPh_2(CH_2)_4PPh_2$), while the decarbonylative coupling product (i.e., spirocycles) was generated in the $P(C_6F_5)_3$-assited system. To explain this interesting selectivity, density functional theory (DFT) calculations have been carried out in the present study. It was found that the direct and decarbonylative couplings experience the same C(acyl)−C(sp^2) activation and alkene insertion steps. The following C−C reductive elimination or β-H elimination−decarbonylation−reductive elimination leads to the direct or decarbonylative coupling reaction, respectively. The coordination features of different ligands were found to significantly influence C−C reductive elimination and decarbonylation step. The requisite phosphine dissociation of DPPB ligand from Rh center for the decarbonylation step is disfavored, and thus, the reductive elimination and direct coupling reaction are favored therein. By contrast, a free coordination site is available on the Rh center in the $P(C_6F_5)_3$-assisted system, facilitating the decarbonylation process together with the generation of related decarbonylative coupling product.

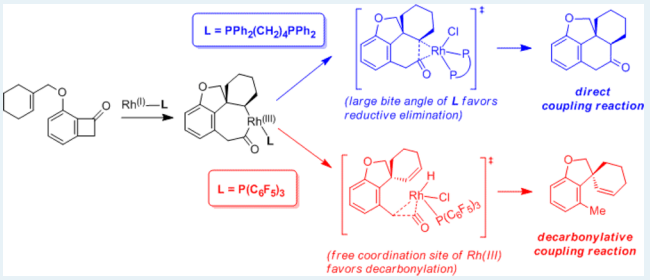

KEYWORDS: *DFT, Rh(I) catalysis, ligand-controlled selectivity, C−C activation, benzocyclobutenone*

1. INTRODUCTION

Transition-metal-catalyzed carbon−carbon bond activation/functionalization are important transformations in organic synthesis due to their great potential in developing significant molecular structures.[1] Despite carbon−carbon bond activation being quite challenging, great progress has been gained with the aid of transition-metal-catalysts.[2] For example, C−CN bond cleavage of nitrile derivatives[3] and functional-group-directed C−C activation[4] have been successfully achieved. In addition, the ring opening process of strained ring compounds also represents an efficient strategy, which is driven by releasing the tension of strained rings.[5] In this context, the catalytic ring expansions of four-membered rings (e.g., cyclobuanol,[6] cyclobutanone[7]) have attracted intensive attention, because these transformations contribute to reconstructing novel carbon frameworks. In 2012, Dong's group reported a $[Rh(COD)Cl]_2$/DPPB-catalyzed (COD = cycloocta-1,5-diene) alkene carboacylation reaction via carbon−carbon bond cleavage of alkene-benzocyclobutenone (**1**) generating the direct coupling product (**2**, Scheme 1).[8] Interestingly, their other study revealed that the decarbonylative coupling products (**3-a** or **3-b**) are formed when choosing $[Rh(CO)_2Cl]_2/P(C_6F_5)_3$ as the catalyst.[9] Furthermore, the yield of olefin-migrated product **3-b** (C3-product) is superior to **3-a** (C2-product) for most substrates (such as cycloheptene-benzocyclobutenone and cyclooctene-benzocyclobutenone), while **3-a** is the main product for only a few cases (such as cyclododecene-benzocyclobutenone).

A plausible mechanism has been proposed by Dong et al.[8,9] As shown in Figure 1, both the direct and decarbonylative coupling reactions start with the oxidative addition of the C(acyl)−C(sp^2) bond of alkene-benzocyclobutenone (**1**). The formed Rh(III) intermediate **A** goes through alkene insertion to produce the metallacycloheptane complex **B**. From **B**, two possible pathways might occur. On one hand, C−C reductive elimination occurs directly on **B** and then gives the direct coupling product **2**. On the other hand, **B** goes through β-H elimination and decarbonylation with the generation of spiro complex **C**, which then undergoes reductive elimination to form the decarbonylative coupling product **3-a**. Besides, the experimental investigations suggested that C2 (**3-a** in Scheme 1) and C3 isomers (**3-b** in Scheme 1) are generated independently, because olefin isomerization does not occur in the decarbonylative coupling products.[9]

Despite of the above proposals, details of the direct and decarbonylative coupling mechanisms (e.g., the rate-determin-

Received: April 30, 2015
Revised: July 2, 2015
Published: July 6, 2015

DOI: 10.1021/acscatal.5b00891
ACS Catal. 2015, 5, 4881−4889

Scheme 1. Rh(I)-Catalyzed Intramolecular Coupling Reactions of Alkene-benzocyclobutenone (1)

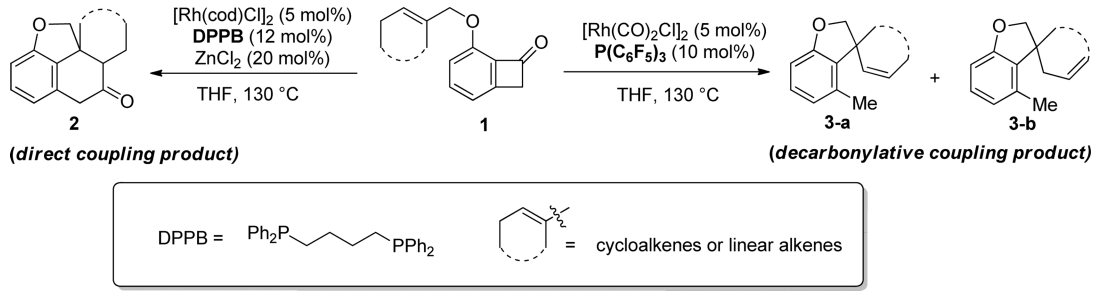

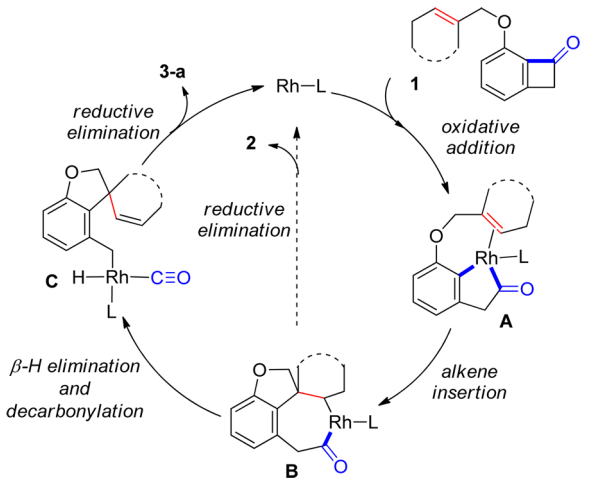

Figure 1. Proposed mechanisms of Rh(I)-catalyzed intramolecular coupling reactions of alkene-benzocyclobutenone (**1**).

ing step, the sequences of β-H elimination, and decarbonylation step in the decarbonylative coupling mechanism) are still unclear. In addition, the detailed olefin migration process in the decarbonylative coupling reaction is barely known. What's more important, the origin of ligand-controlled selectivity remains to be explained. To settle these problems, we studied the Rh(I)-catalyzed direct and decarbonylative coupling mechanisms of alkene-benzocyclobutenone by DFT methods. Our computational results corroborate Dong's previous proposals on the overall mechanisms. To be specific, the direct and decarbonylative coupling mechanisms undergo the same oxidative addition and alkene insertion steps. Then the subsequent C−C reductive elimination or β-H elimination-decarbonylation-reductive elimination leads to the direct or decarbonylative coupling mechanisms, respectively. To be noted, intramolecular Rh−H addition−elimination mechanism (instead of π-allyl pathway[10]) is responsible for the generation of olefin-migrated decarbonylative coupling product. Furthermore, bidentate structure of DPPB is the key to facilitate C−C reductive elimination over competitive decarbonylation step, because the prerequisite partial dissociation of DPPB from Rh(III) center (in the decarbonylation step) is highly disfavored. Therefore, the direct coupling reaction is preferred for DPPB-assisted system. In contrast, the free coordination site on the Rh center facilitates the decarbonylation step in the presence of $P(C_6F_5)_3$ ligand and, then, leads to the priority of decarbonylative coupling reaction.

2. COMPUTATIONAL METHODS

All the calculations were conducted with Gaussian 09 software.[11] The B3LYP functional[12] was used for the gas-phase geometry optimization of all species. The LANL2DZ basis set[13] was employed for Rh, and the 6-31G(d) basis set was used for the other atoms (GEN1). At the B3LYP/GEN1 level, frequency analysis was performed to ensure the stationary point as minimum or transition state. The IRC calculation[14] was applied for each transition state to confirm that it connects the right reactant and product. For the solvent effect, the single-point calculation on the gas-phase optimized geometry with SMD solvation model[15] (solvent = tetrahydrofuran) was applied. The single-point calculation was carried out by using M06[16] with GEN2 (i.e., LANL2DZ with additional polarization function $\zeta(f) = 1.350$[17] for Rh, and 6-311+G(d,p) for the rest of atoms). This M06//B3LYP computational method has been widely employed in Rh catalytic reactions.[18] Solution-phase single-point energy corrected by gas-phase Gibbs free energy correction was used for the reported energy in this study.

3. RESULTS AND DISCUSSION

In this study, the coupling reactions of cyclohexene-benzocyclobutenone (**reactant**) in the presence of Rh(I) catalyst and $P(C_6F_5)_3$ or DPPB ligand were chosen as model reactions eqs 1 and 2. For $P(C_6F_5)_3$-assisted system, three types of products (including **prod1-c2**, **prod1-c3**, and **prod2**) are obtained and the olefin-migrated spirocycle **prod1-c3** is the major product. While the direct coupling product **prod2** is the

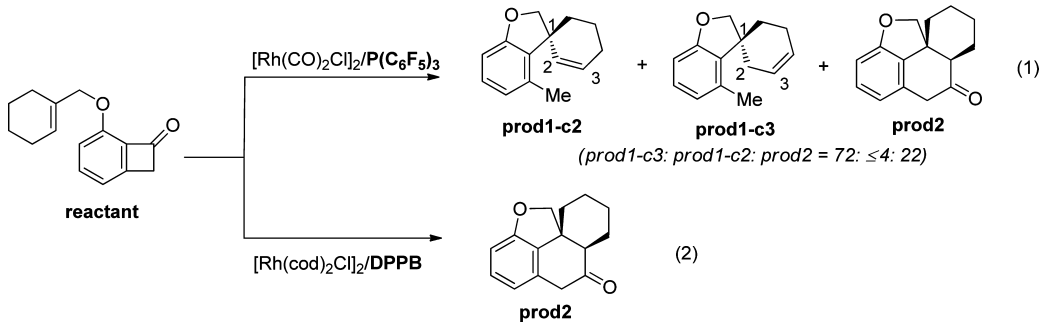

DOI: 10.1021/acscatal.5b00891
ACS Catal. 2015, 5, 4881−4889

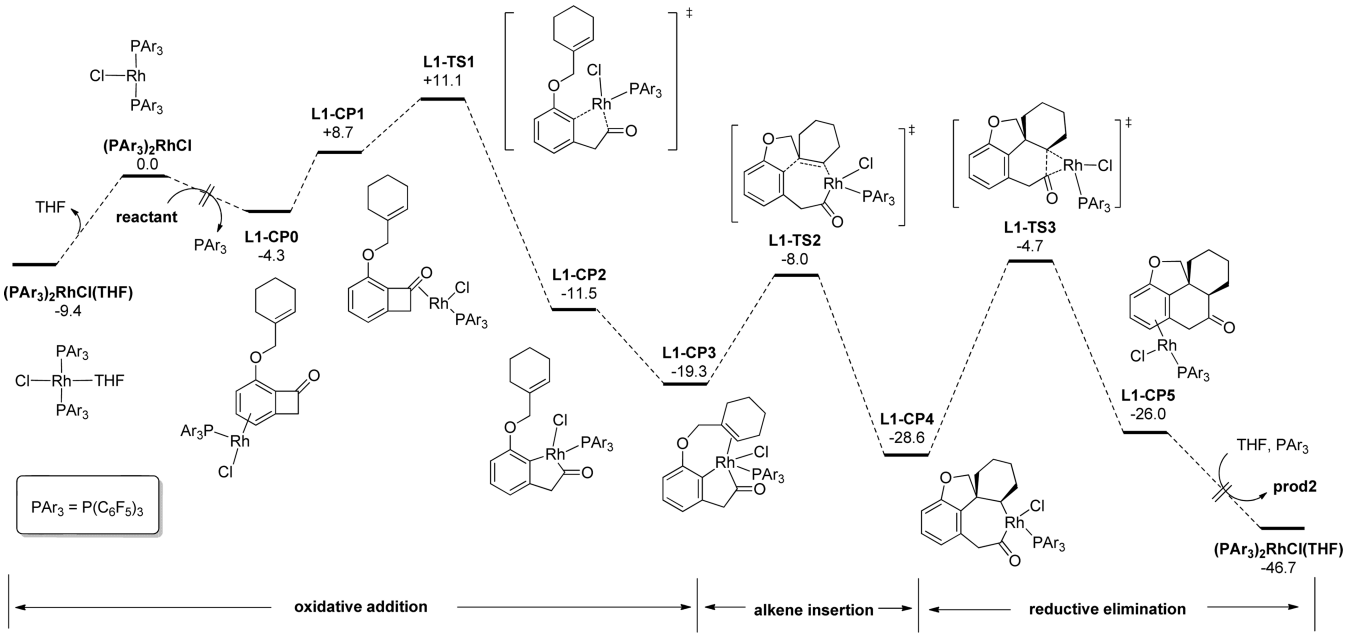

Figure 2. Energy profiles of the direct coupling mechanism of eq 1.

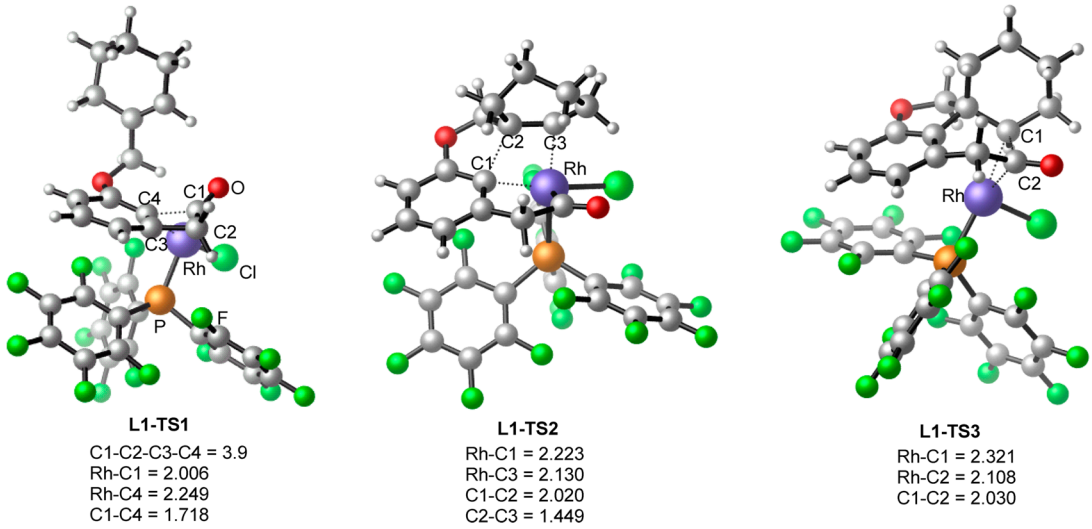

Figure 3. Optimized structures of **L1-TS1**, **L1-TS2**, and **L1-TS3**. Bond lengths are given in angstroms. Dihedral angles are shown in degrees.

sole product for DPPB-assisted system (Note that **prod1-c2**, **prod1-c3**, and **prod2** correspond to the product types of **3-a**, **3-b**, and **2** in Scheme 1, respectively).

3.1. Mechanisms with $P(C_6F_5)_3$ Ligand. In this section, we first studied the $[Rh(CO)_2Cl]_2/P(C_6F_5)_3$ catalyzed direct coupling mechanism of **reactant** to **prod2**. Then decarbonylative coupling mechanisms for the formation of **prod1-c2** and its isomer **prod1-c3** were explored.

3.1.1. Direct Coupling Mechanism. Energy profiles of the direct coupling mechanism of eq 1 are shown in Figure 2 and the optimized structures of related transition states are shown in Figure 3.

The catalytic cycle starts with the THF-coordinated catalyst **$(PAr_3)_2RhCl(THF)$**, which dissociates THF to generate active catalyst **$(PAr_3)_2RhCl$** (i.e., the energetic reference point of eq 1). **$(PAr_3)_2RhCl$** loses one molecule of PAr_3 ligand, and coordinates with benzene group of reactant to form the stable complex **L1-CP0**. **L1-CP0** then isomerizes to the precursor of oxidative addition **L1-CP1**, this step is endergonic by 13.0 kcal/mol. From **L1-CP1**, oxidative addition of the C(acyl)−C(sp^2) bond via transition state **L1-TS1** produces the C(acyl)−Rh(III) intermediate **L1-CP2** with an energy barrier of +15.4 kcal/mol. It is noted that alkene does not act as the directing group to activate the C(acyl)−C(sp^2) bond, because the steric effects between phosphine ligand and cyclohexene make Rh center locate below the C1−C2−C3−C4 plane (Figure 3).[19] From **L1-CP2**, isomerization occurs to generate the alkene-coordinated complex **L1-CP3**, from which alkene insertion via **L1-TS2** requires an energy barrier of 11.3 kcal/mol (**L1-CP3** → **L1-TS2**). The subsequent reductive elimination on **L1-CP4** occurs via transition state **L1-TS3** to give the product-coordinated complex **L1-CP5**. In **L1-TS3**, the Cl atom locates adjacent to the phosphine ligand, and the Rh(III) center lies below the cyclohexane plane (as shown in Figure 3). Finally the ligand exchange between THF, PAr_3 and **L1-CP5** delivers the direct coupling product **prod2** and regenerates **$(PAr_3)_2RhCl$**-

DOI: 10.1021/acscatal.5b00891
ACS Catal. 2015, 5, 4881−4889

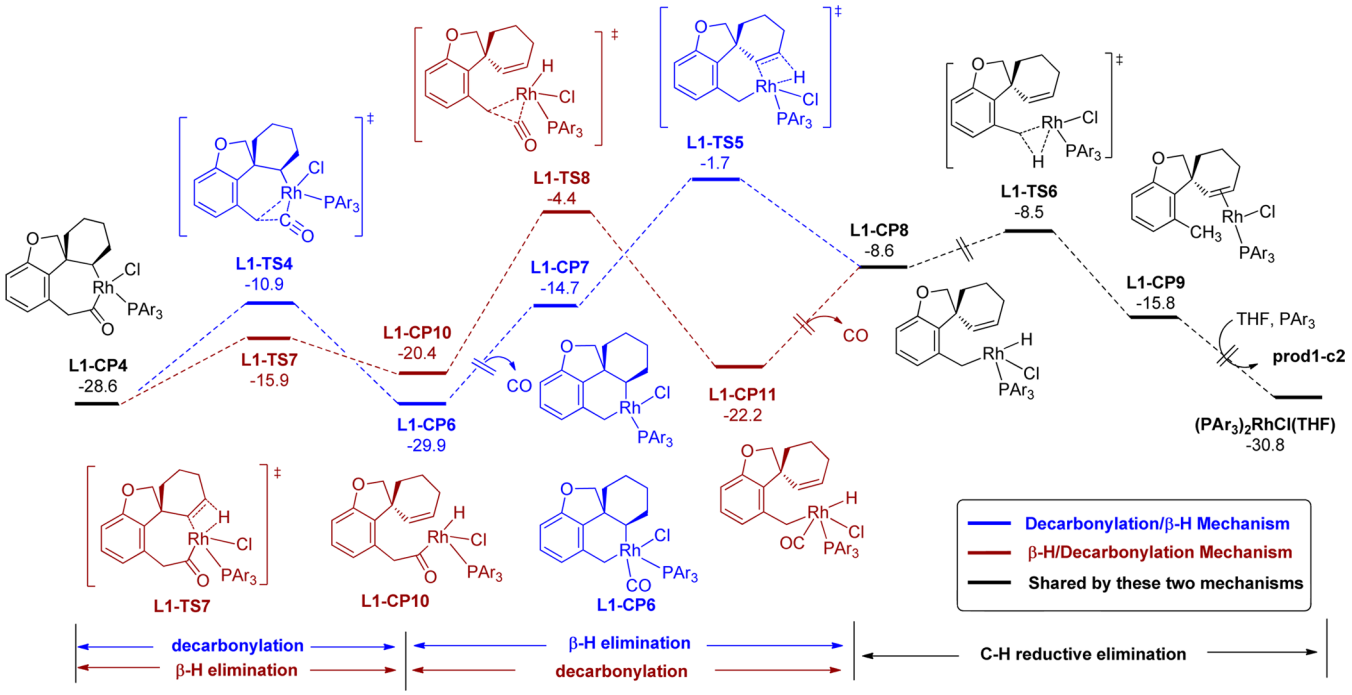

Figure 4. Energy profiles of the decarbonylation/β-H mechanism (blue line) and β-H/decarbonylation mechanism (red line) of eq 1.

(**THF**). According to Figure 2, reductive elimination (**L1-CP4** → **L1-TS3**, $\Delta G^{\ddagger}$ = +23.9 kcal/mol) is the rate-determining step of direct coupling mechanism of eq 1.

3.1.2. Decarbonylative Coupling Mechanisms. Decarbonylation/β-H Mechanism. For the decarbonylative coupling mechanism, we examined two possible pathways regarding the different sequences of decarbonylation and β-H elimination steps: Decarbonylation/β-H mechanism (decarbonylation occurs before β-H elimination) and β-H/decarbonylation mechanism (decarbonylation occurs after β-H elimination). Herein, we started with decarbonylation/β-H mechanism, in which the product of alkene insertion (i.e., **L1-CP4**) experiences the decarbonylation, β-H elimination and reductive elimination steps successively. As shown in Figure 4 (blue line), from **L1-CP4**, decarbonylation occurs via the three-centered transition state **L1-TS4** and delivers CO-coordinated product **L1-CP6**.[20] Then CO dissociates from Rh(III) of **L1-CP6** to provide a vacant site for the following β-H elimination step. The resulting **L1-CP7** goes through β-H elimination to produce spirocyclic intermediate **L1-CP8**. The β-H elimination step (**L1-CP6** → **L1-TS5** → **L1-CP8**) needs to overcome an energy barrier of +28.2 kcal/mol and is endergonic by 21.3 kcal/mol. Then a facile C−H reductive elimination occurs to give product-coordinated complex **L1-CP9**, which exchanges with THF and PAr_3 to form **prod1-c2**.

β-H/Decarbonylation Mechanism. We also studied the β-H/Decarbonylation Mechanism, in which **L1-CP4** successively undergoes β-H elimination, decarbonylation, and reductive elimination steps (Figure 4, red line). In detail, **L1-CP4** goes through β-H elimination transition state **L1-TS7** to generate acyl-Rh(III)-H intermediate **L1-CP10**. This step requires an energy barrier of +12.7 kcal/mol (**L1-CP4** → **L1-TS7**). Thereafter, decarbonylation occurs on **L1-CP10** via **L1-TS8** (ΔG = −4.4 kcal/mol) to form the CO-coordinated intermediate **L1-CP11**. Then dissociation of CO from **L1-CP11** produces **L1-CP8**, from which C−H reductive elimination occurs via the same way as the decarbonylation/β-H mechanism (**L1-CP8** → **L1-TS6** → **L1-CP9**).

According to the above computational results, the rate-determining step of decarbonylation/β-H mechanism is β-H elimination step with an overall energy barrier of +28.2 (**L1-CP6** → **L1-TS5**). By contrast, the rate-determining step of β-H/decarbonylation mechanism is decarbonylation step, and its overall energy barrier is +24.2 kcal/mol (**L1-CP4** → **L1-TS8**). The inferiority of the decarbonylation/β-H mechanism results from its difficult CO dissociation process. While the facile decarbonylation from acyl-Rh(III)-H intermediate (i.e., **L1-CP10**) makes β-H/decarbonylation mechanism as the more plausible decarbonylative coupling mechanism.[21]

3.1.3. Mechanistic Explanation of Olefin Migration. The above discussions figure out pathways delivering the direct coupling product **prod2** (section 3.1.1) and decarbonylative coupling product **prod1-c2** (section 3.1.2), while the mechanistic interpretation of olefin-migrated product **prod1-c3** remains unclear. As the possibility for the transformation of **prod1-c2** to **prod1-c3** has been ruled out by both experimental observations and our calculations,[22] herein we mainly focus on other possible pathways for olefin migration.

For transition-metal catalyzed olefin migration, two possible mechanisms have been examined. As shown in Scheme 2, the most commonly accepted one is the M−H addition−elimination mechanism,[23] which is initiated by adding the M−H species to the double bond of olefin. Then the resultant alkyl−M complex goes through β-H elimination to complete olefin migration (Scheme 2a). An alternative mechanism involves the generation of π-allyl intermediate, resulting in the 1,3-H shift process (Scheme 2b).[10] The details of both M−H addition−elimination and π-allyl mechanisms in the concerned Rh-catalyzed decarbonylative coupling reaction were explored. Since the energy barrier of π-allyl mechanism[24] is 9.9 kcal/mol higher than that of the Rh−H addition−elimination mechanism, only the energy profiles of the

DOI: 10.1021/acscatal.5b00891
ACS Catal. 2015, 5, 4881−4889

Scheme 2. Two Possible Mechanisms of Olefin Migration

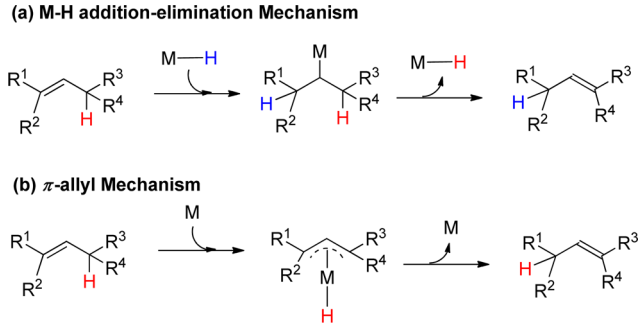

preferred Rh−H addition−elimination mechanism are given here for clarity (Figures 5 and 6).[25]

Starting from acyl-Rh(III)−H intermediate **L1-CP10**, migration insertion via **L1-TS9** gives the metallacyclooctane complex **L1-CP12** with 2.9 kcal/mol energy barrier. Thereafter, **L1-CP12** experiences a facile β-H elimination step through **L1-TS10** (ΔG = −16.6 kcal/mol) to produce the olefin-migrated acyl-Rh(III)−H complex **L1-CP13**. The following decarbonylation from **L1-CP13** via **L1-TS11** requires an energy barrier of 13.5 kcal/mol. The resulting intermediate **L1-CP14** then dissociates CO and undergoes C−H reductive elimination to give the product-coordinated complex **L1-CP15**. Herein, it is interesting to note that the energy barrier for reductive elimination from **L1-CP14** is comparable to that of **L1-CP11** (+15.3 vs +13.7 kcal/mol), due to the similar coordination environment of the rhodium center. Finally, olefin-migrated product **prod1-c3** is generated through ligand exchange between THF, PAr_3 and **L1-CP15**.

3.1.4. Overview of the Mechanisms of Equation 1. To further understand the mechanistic differences among these three products of eq 1 (i.e., **prod1-c2**, **prod1-c3**, and **prod2**), we concluded the above studied mechanisms in Scheme 3. The first two steps in the mechanisms of these products are the same, including oxidative addition and alkene insertion. From the product of alkene insertion (i.e., seven-membered-ring rhodacycle) there are different possible pathways. On one hand, C−C reductive elimination would generate direct coupling product **prod2**. On the other hand, β-H elimination could give acyl-Rh(III)−H complex, which is followed by decarbonylation and reductive elimination to produce **prod1-c2**. Besides, olefin migration (see Figure 5 for details) might occur on the acyl-Rh(III)−H complex to generate olefin-migrated acyl-Rh(III)−H complex, and then, **prod1-c3** is finally obtained.

Comparing the above three pathways, we found that the rate-determining steps of both **prod1-c2** and **prod1-c3** are decarbonylation step, while the rate-determining step of **prod2** is reductive elimination. The energy barriers of **prod1-c2**, **prod1-c3**, and **prod2** are +24.2, +23.5, and +23.9 kcal/mol, respectively. Considering the uncertainties of computational methods, we suggested that all these pathways are competitive for the Rh/$P(C_6F_5)_3$ catalyst system.[26]

3.2. Mechanism with DPPB Ligand. Similar to the aforementioned discussions on Rh(I)/$P(C_6F_5)_3$ catalyst system, we started studying the direct coupling mechanism of Rh/DPPB-catalyzed coupling reaction of cyclohexene-benzocyclobutenone (Figure 7).

First, active catalyst **(dppb)RhCl** is generated through dissociating THF molecule from **(dppb)RhCl(THF)**. Then oxidative addition of C(sp^2)−C(acyl) of **reactant** occurs via transition state **L2-TS1** to give the Rh(III) complex **L2-CP1**. The energy barrier of oxidative addition is +21.9 kcal/mol with releasing 12.2 kcal/mol free energy. Because the following alkene insertion step requires the coordination of intramolecular alkene to Rh(III) center, dissociation of one arm of DPPB ligand (−PPh_2) from Rh(III) center is necessary to provide a vacant site.[27] This partial ligand dissociation process from **L2-CP1** to **L2-CP2** is endergonic by 14.6 kcal/mol. From **L2-CP2**, alkene insertion via **L2-TS2** requires the energy barrier of +19.9 kcal/mol.[28] Then DPPB ligand of the formed **L2-CP3** recovers its bidentate structure to form **L2-CP4**, from which reductive elimination via **L2-TS3** (ΔG = +12.8 kcal/mol) generates the direct coupling product **prod2**. From Figure 7, the rate-determining step of direct coupling mechanism of eq 2 is alkene insertion, and the overall energy barrier is +34.5 kcal/mol (**L2-CP1** → **L2-TS2**).

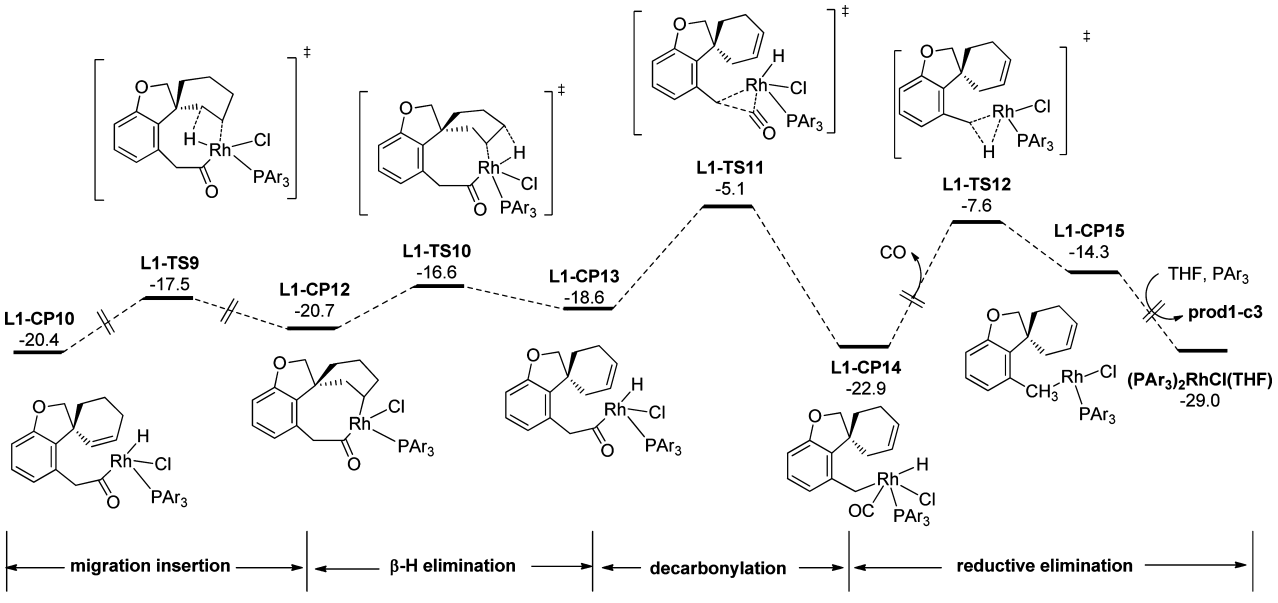

Figure 5. Energy profiles of intramolecular Rh−H addition−elimination mechanism of eq 1.

DOI: 10.1021/acscatal.5b00891
ACS Catal. 2015, 5, 4881−4889

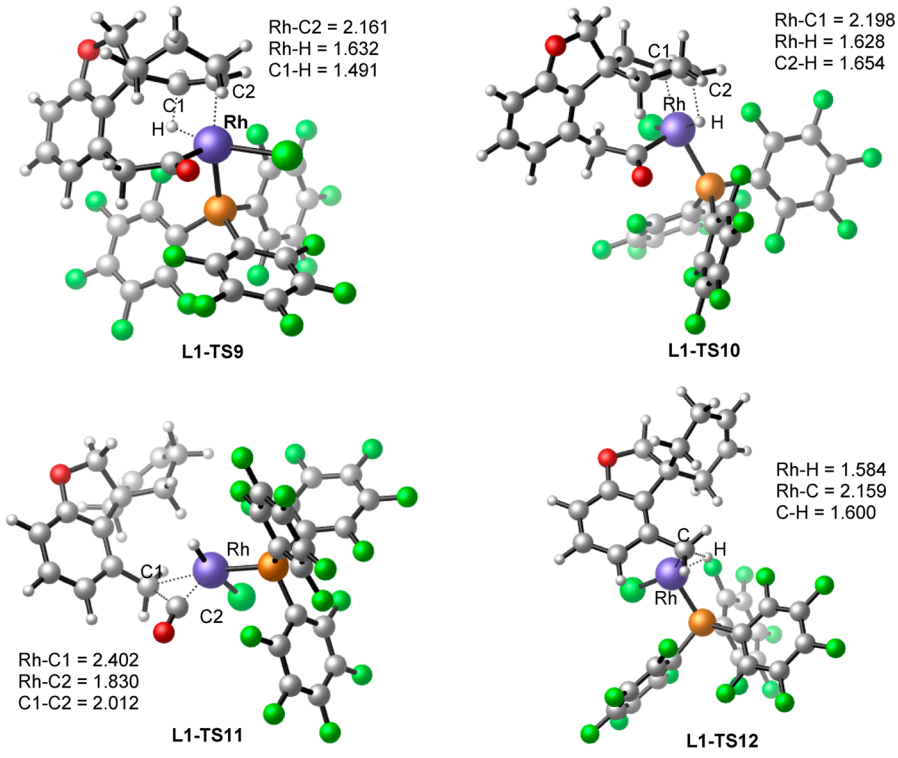

Figure 6. Optimized structures of transition states involved in Figure 5. Bond lengths are shown in angstroms.

Scheme 3. Three Possible Pathways for Rh(I)/P(C_6F_5)$_3$-Catalyzed Coupling Reaction of Cyclohexene-benzocyclobutenones

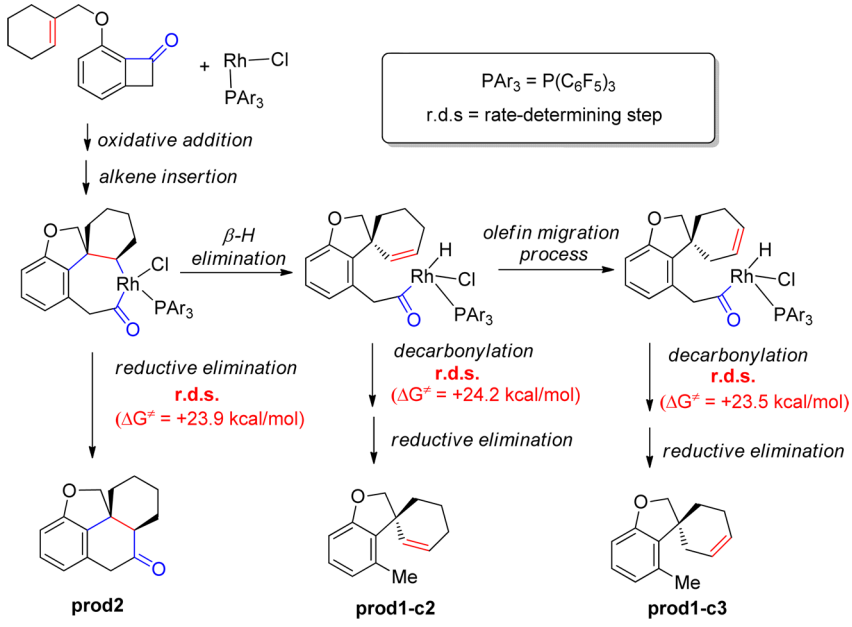

The possibility of decarbonylative coupling mechanism was also considered. The computational results indicate that **L2-CP3** would undergo decarbonylation transition state **L2-TS4** to complete the β-H/decarbonylation mechanism. Because the energy of **L2-TS4** (ΔG = +20.0 kcal/mol) is higher than that of **L2-TS3** (ΔG = +12.8 kcal/mol), decarbonylative coupling reaction is unlikely for eq 2. In other words, direct coupling reaction in generation of **prod2** is preferred for DPPB-assisted system, which agrees with the experiment results.

To be noted, we also investigated the impact of $ZnCl_2$ on the DPPB-assisted mechanisms. It was found that $ZnCl_2$ significantly promotes the direct coupling reaction, while hindering the decarbonylative coupling reaction. This is in accordance with the experimental results that involvement of $ZnCl_2$ leads to high yields of direct coupling products (please see the Supporting Information for more details).

3.3. Origin of Selectivity. According to the aforementioned calculation results, the decarbonylation process (**L1-TS11**, ΔG = −5.1 kcal/mol) is slightly favored over C−C reductive elimination step (**L1-TS3**, ΔG = −4.7 kcal/mol) in the P(C_6H_5)$_3$-assisted system eq 1; therefore, the decarbonylative coupling mechanism is more favored. By contrast,

DOI: 10.1021/acscatal.5b00891
ACS Catal. 2015, 5, 4881−4889

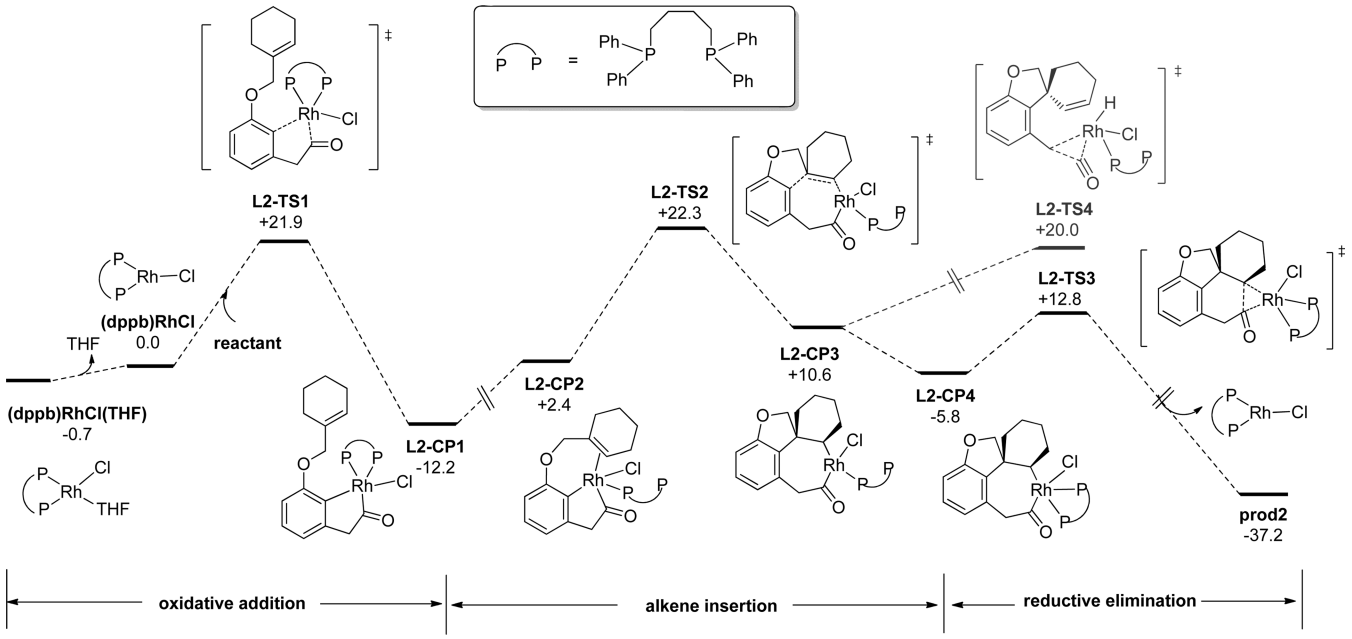

Figure 7. Energy profiles of Rh(I)/DPPB catalyzed coupling reaction of cyclohexene-benzocyclobutenones.

Scheme 4. Comparison between the Reductive Elimination and Decarbonylation Steps: (a) $P(C_6H_5)_3$-Assisted System and (b) DPPB-Assisted Systems

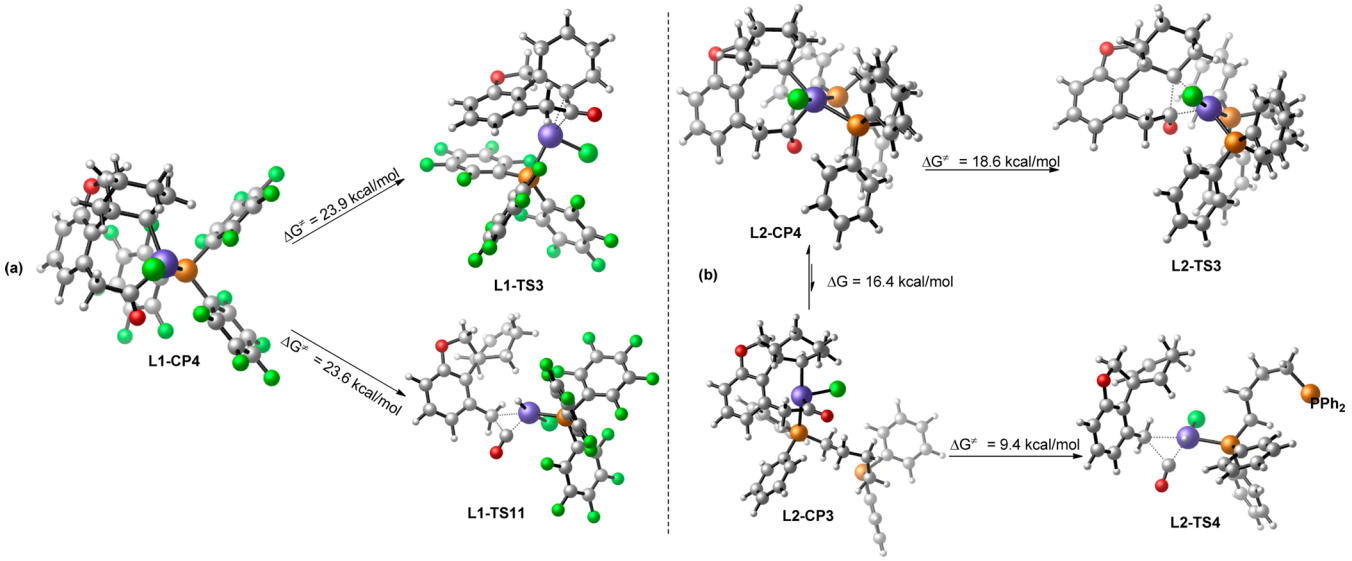

reductive elimination (**L2-TS3**, ΔG = +12.8 kcal/mol) is more likely to happen than decarbonylation process (**L2-TS4**, ΔG = +20.0 kcal/mol) in the DPPB-assisted reaction, resulting in the feasible direct coupling mechanism. Then we made an effort to understand how different ligands affect the reductive elimination and decarbonylation step.[29]

As shown in Scheme 4, both the reductive elimination and decarbonylation steps involving DPPB ligand are relatively easier than the related ones with $P(C_6H_5)_3$ ligand. In details, the energy barrier of reductive elimination of **L2-CP4** (**L2-CP4** → **L2-TS3**, $\Delta G^{\ddagger}$ = 18.6 kcal/mol) is 5.3 kcal/mol lower than that of **L1-CP4** (**L1-CP4** → **L1-TS3**, $\Delta G^{\ddagger}$ = 23.9 kcal/mol), resulting from the large bite angle of DPPB ligand in reductive elimination.[30] Besides, decarbonyaltion of **L2-CP3** (**L2-CP3** → **L2-TS4**, $\Delta G^{\ddagger}$ = 9.4 kcal/mol) is more preferred than **L1-CP4** (**L1-CP4** → **L1-TS11**, $\Delta G^{\ddagger}$ = 23.5 kcal/mol), owing to the smaller steric effects of partial-dissociated DPPB ligand. However, the ligand dissociation process (**L2-CP4** → **L2-CP3**) in DPPB-assisted system is requisite to provide a vacant site for the following decarbonylation process. This ligand dissociation process involves the distortion of bidentate structure of DPPB ligand and causes the decrease of electron density of the Rh(III) center (the NBO charge of Rh varies from −0.390 to −0.119). Thus, dissociation of DPPB to the detrimental monodentate coordination mode is highly endergonic by 16.4 kcal/mol, which accordingly increases the energy barrier of decarbonylation step from 9.4 (**L2-CP3** → **L2-TS4**) to 25.8 kcal/mol (**L2-CP4** → **L2-TS4**). Consequently, reductive elimination is superior to decarbonylation process for DPPB-assisted system, and this promotes the direct coupling reaction. On the contrary, in $P(C_6H_5)_3$-assisted system, the vacant coordination site on Rh center benefits

DOI: 10.1021/acscatal.5b00891
ACS Catal. 2015, 5, 4881−4889

decarbonylation process. Therefore, decarbonylative coupling reaction is preferred for $P(C_6H_5)_3$-assisted system.

4. CONCLUSION

Recently, Dong et al. described the intramolecular coupling reactions of alkene-benzocyclobutenones: the direct coupling products (i.e., polyfused ring systems) are favored with the bidentate DPPB ligand, while the decarbonylative coupling products (i.e., spirocycles) were gained with the monodentate ligand $P(C_6F_5)_3$. To explain this ligand-controlled selectivity, we studied the direct and decarbonylative coupling mechanisms of cyclohexene-benzocyclobutenone by means of DFT methods.

The calculation results indicate that direct and decarbonylative coupling mechanisms undergo the same oxidative addition and alkene insertion steps. Thereafter, the C−C reductive elimination leads to direct coupling mechanism. On the other hand, the decarbonylative coupling mechanism proceeds via the β-H elimination, decarbonylation and C−H reductive elimination steps (β-H/decarbonylation mechanism). Herein, the β-H elimination precedes decarbonylation step, because the dissociation of CO from six-membered-ring rhodacycle is disfavored when decarbonylation occurs prior to β-H elimination step. The experimentally observed selectivity on different products (i.e., polyfused ring or spirocycles) was well reproduced by the computational results. In addition, the intramolecular Rh−H addition−elimination pathway is critical to olefin migration in decarbonylative coupling reaction, and this accords with the independent generation of C2 and C3 olefin isomers.

On the basis of the above mechanistic details, the origin of ligand-controlled selectivity has been analyzed. It was found that ligand-controlled selectivity depends on the relative feasibility of C−C reductive elimination (in direct coupling mechanism) and decarbonylation step (in decarbonylative coupling mechanism). For DPPB-assisted system, decarbonylation step requires the energetically unfavorable partial dissociation of DPPB ligand, which leads to the advantage of direct C−C reductive elimination step. Therefore, DPPB-assisted system facilitates the direct coupling reaction. On the contrary, the ligand dissociation process is unnecessary for $P(C_6F_5)_3$-assisted system, and thus the decarbonylative coupling reaction is relatively more favorable.

■ ASSOCIATED CONTENT

Supporting Information

The Supporting Information is available free of charge on the ACS Publications website at DOI: 10.1021/acscatal.5b00891.

Cleavage of C(acyl)−C(sp^3) of the reactant, the π-allyl mechanism of olefin migration, energies, and Cartesian coordinates of all calculated species (PDF)

■ AUTHOR INFORMATION

Corresponding Authors

*E-mail: fuyao@ustc.edu.cn (Y.F.)
*E-mail: yuhaizhu@gmail.com (H.Y.).

Notes

The authors declare no competing financial interest.

■ ACKNOWLEDGMENTS

We thank the NSFC (21325208, 21172209, 21361140372, 21202006), the 973 Program (2012CB215306), FRFCU (WK2060190025, WK2060190040, FRF-TP-14-015A2), CAS (KJCX2-EW-J02), PCSIRT, and National Supercomputing Center in Shenzhen and USTC for providing the computational resources.

■ REFERENCES

(1) (a) Marek, I.; Masarwa, A.; Delaye, P. O.; Leibeling, M. *Angew. Chem., Int. Ed.* **2015**, *54*, 414−429. (b) Chen, F.; Wang, T.; Jiao, N. *Chem. Rev.* **2014**, *114*, 8613−8661. (c) Ruhland, K. *Eur. J. Org. Chem.* **2012**, *2012*, 2683−2706. (d) Jun, C. H. *Chem. Soc. Rev.* **2004**, *33*, 610−618. (d) Shang, R.; Liu, L. *Sci. China Chem.* **2011**, *54*, 1670−1687. (e) Crabtree, R. H. *Chem. Rev.* **1985**, *85*, 245−269. (f) Rybtchiski, B.; Milstein, D. *Angew. Chem., Int. Ed.* **1999**, *38*, 870−883.

(2) (a) Murphy, S. K.; Park, J.; Cruz, F. A.; Dong, V. M. *Science* **2015**, *347*, 56−60. (b) Li, B. S.; Wang, Y.; Jin, Z.; Zheng, P.; Ganguly, R.; Chi, Y. R. *Nat. Commun.* **2015**, *6*, 6207. (c) Shaw, M. H.; McCreanor, N. G.; Whittingham, W. G.; Bower, J. F. *J. Am. Chem. Soc.* **2015**, *137*, 463−468. (d) Tang, C.; Jiao, N. *Angew. Chem., Int. Ed.* **2014**, *53*, 6528−6532. (e) Youn, S. W.; Kim, B. S.; Jagdale, A. R. *J. Am. Chem. Soc.* **2012**, *134*, 11308−11311.

(3) (a) Minami, Y.; Yoshiyasu, H.; Nakao, Y.; Hiyama, T. *Angew. Chem., Int. Ed.* **2013**, *52*, 883−887. (b) Hirata, Y.; Yukava, T.; Kashihara, N.; Nakao, Y.; Hiyama, T. *J. Am. Chem. Soc.* **2009**, *131*, 10964−10973. (c) Tobisu, M.; Chatani, N. *Chem. Soc. Rev.* **2008**, *37*, 300−307. (d) Tobisu, M.; Kita, Y.; Ano, Y.; Chatani, N. *J. Am. Chem. Soc.* **2008**, *130*, 15982−15989. (e) Tobisu, M.; Kita, Y.; Chatani, N. *J. Am. Chem. Soc.* **2006**, *128*, 8152−8153.

(4) (a) Zeng, R.; Dong, G. *J. Am. Chem. Soc.* **2015**, *137*, 1408−1411. (b) Lei, Z. Q.; Pan, F.; Li, H.; Li, Y.; Zhang, X. S.; Chen, K.; Wang, X.; Li, Y. X.; Sun, J.; Shi, Z. J. *J. Am. Chem. Soc.* **2015**, *137*, 5012−5020. (c) Matsuda, T.; Yuihara, I. *Chem. Commun.* **2015**, *51*, 7393−7396. (d) Shaw, M. H.; Melikhova, E. Y.; Kloer, D. P.; Whittingham, W. G.; Bower, J. F. *J. Am. Chem. Soc.* **2013**, *135*, 4992−4995. (e) Lei, Z. Q.; Li, H.; Li, Y.; Zhang, X. S.; Chen, K.; Wang, X.; Sun, J.; Shi, Z. J. *Angew. Chem., Int. Ed.* **2012**, *51*, 2690−2694. (f) Li, H.; Li, Y.; Zhang, X. S.; Chen, K.; Wang, X.; Shi, Z. J. *J. Am. Chem. Soc.* **2011**, *133*, 15244−15247. (g) Dreis, A. M.; Douglas, C. J. *J. Am. Chem. Soc.* **2009**, *131*, 412−413. (h) Shang, R.; Yang, Z.-W.; Wang, Y.; Zhang, S.-L.; Liu, L. *J. Am. Chem. Soc.* **2010**, *132*, 14391−14393.

(5) (a) Mack, D. J.; Njardarson, J. T. *ACS Catal.* **2013**, *3*, 272−286. (b) Seiser, T.; Saget, T.; Tran, D. N.; Cramer, N. *Angew. Chem., Int. Ed.* **2011**, *50*, 7740−7752. (c) Shi, M.; Shao, L. X.; Lu, J. M.; Wei, Y.; Mizuno, K.; Maeda, H. *Chem. Rev.* **2010**, *110*, 5883−5913. (d) Rubin, M.; Rubina, M.; Gevorgyan, V. *Chem. Rev.* **2007**, *107*, 3117−3179. (e) Namyslo, J. C.; Kaufmann, D. E. *Chem. Rev.* **2003**, *103*, 1485−1537.

(6) (a) Xia, Y.; Liu, Z.; Ge, R.; Ye, F.; Hossain, M.; Zhang, Y.; Wang, J.; Liu, Z. *J. Am. Chem. Soc.* **2014**, *136*, 3013−3015. (b) Souillart, L.; Cramer, N. *Chem. Sci.* **2014**, *5*, 837−840. (c) Seiser, T.; Cramer, N. *J. Am. Chem. Soc.* **2010**, *132*, 5340−5341. (d) Seiser, T.; Roth, O. A.; Cramer, N. *Angew. Chem., Int. Ed.* **2009**, *48*, 6320−6323. (e) Ding, L.; Ishida, N.; Murakami, M.; Morokuma, K. *J. Am. Chem. Soc.* **2014**, *136*, 169−178.

(7) (a) Souillart, L.; Parker, E.; Cramer, N. *Angew. Chem., Int. Ed.* **2014**, *53*, 3001−3005. (b) Souillart, L.; Cramer, N. *Angew. Chem., Int. Ed.* **2014**, *53*, 9640−9644. (c) Ko, H. M.; Dong, G. *Nat. Chem.* **2014**, *6*, 739−744. (d) Matsuda, T.; Shigeno, M.; Murakami, M. *J. Am. Chem. Soc.* **2007**, *129*, 12086−12087. (e) Murakami, M.; Ashida, S. *Chem. Commun.* **2006**, 4599−4601. (f) Murakami, M.; Ashida, S.; Matsuda, T. *J. Am. Chem. Soc.* **2005**, *127*, 6932−6933.

(8) Xu, T.; Dong, G. *Angew. Chem., Int. Ed.* **2012**, *51*, 7567−7571.

(9) Xu, T.; Savage, N. A.; Dong, G. *Angew. Chem., Int. Ed.* **2014**, *53*, 1891−1895.

(10) For selected examples of π-allyl mechanism of olefin migration process, see: (a) Biswas, S.; Huang, Z.; Choliy, Y.; Wang, D. Y.; Brookhart, M.; Krogh-Jespersen, K.; Goldman, A. S. *J. Am. Chem. Soc.* **2012**, *134*, 13276−13295. (b) Knapp, S. M. M.; Shaner, S. E.; Kim, D.;

DOI: 10.1021/acscatal.5b00891
ACS Catal. 2015, 5, 4881−4889

Shpov, D. Y.; Tendler, J. A.; Pudalov, D. M.; Chianese, A. R. *Organometallics* **2014**, *33*, 473−484. (c) Stefani, A.; Consiglio, G.; Botteghi, C.; Pino, P. *J. Am. Chem. Soc.* **1977**, *99*, 1058−1063. (d) Harrod, J. F.; Chalk, A. J. *J. Am. Chem. Soc.* **1966**, *88*, 3491−3497.
(11) Frisch, M. J.; Trucks, G. W.; Schlegel, H. B.; Scuseria, G. E.; Robb, M. A.; Cheeseman, J. R.; Scalmani, G.; Barone, V.; Mennucci, B.; Petersson, G. A.; Nakatsuji, H.; Caricato, M.; Li, X.; Hratchian, H. P.; Izmaylov, A. F.; Bloino, J.; Zheng, G.; Sonnenberg, J. L.; Hada, M.; Ehara, M.; Toyota, K.; Fukuda, R.; Hasegawa, J.; Ishida, M.; Nakajima, T.; Honda, Y.; Kitao, O.; Nakai, H.; Vreven, T.; Montgomery, J. A., Jr.; Peralta, J. E.; Ogliaro, F.; Bearpark, M.; Heyd, J. J.; Brothers, E.; Kudin, K. N.; Staroverov, V. N.; Keith, T.; Kobayashi, R.; Normand, J.; Raghavachari, K.; Rendell, A.; Burant, J. C.; Iyengar, S. S.; Tomasi, J.; Cossi, M.; Rega, N.; Millam, J. M.; Klene, M.; Knox, J. E.; Cross, J. B.; Bakken, V.; Adamo, C.; Jaramillo, J.; Gomperts, R.; Stratmann, R. E.; Yazyev, O.; Austin, A. J.; Cammi, R.; Pomelli, C.; Ochterski, J. W.; Martin, R. L.; Morokuma, K.; Zakrzewski, V. G.; Voth, G. A.; Salvador, P.; Dannenberg, J. J.; Dapprich, S.; Daniels, A. D.; Farkas, O.; Foresman, J. B.; Ortiz, J. V.; Cioslowski, J.; Fox, D. J. *Gaussian 09*, revision D.01; Gaussian, Inc.: Wallingford CT, 2013.
(12) (a) Miehlich, B.; Savin, A.; Stoll, H.; Preuss, H. *Chem. Phys. Lett.* **1989**, *157*, 200−206. (b) Lee, C. T.; Yang, W. T.; Parr, R. G. *Phys. Rev. B* **1988**, *37*, 785−789.
(13) Wadt, W. R.; Hay, P. J. *J. Chem. Phys.* **1985**, *82*, 284−298.
(14) (a) Fukui, K. *Acc. Chem. Res.* **1981**, *14*, 363−368. (b) Fukui, K. *J. Phys. Chem.* **1970**, *74*, 4161−4163.
(15) Marenich, A. V.; Cramer, C. J.; Truhlar, D. G. *J. Phys. Chem. B* **2009**, *113*, 6378−6396.
(16) Zhao, Y.; Truhlar, D. G. *Theor. Chem. Acc.* **2008**, *120*, 215−241.
(17) Ehlers, A. W.; Bohme, M.; Dapprich, S.; Gobbi, A.; Hollwarth, A.; Jonas, V.; Kohler, K. F.; Stegmann, R.; Veldkamp, A.; Frenking, G. *Chem. Phys. Lett.* **1993**, *208*, 111−114.
(18) (a) Lin, M.; Kang, G. Y.; Guo, Y. A.; Yu, Z. X. *J. Am. Chem. Soc.* **2012**, *134*, 398−405. (b) Jiang, Y.-Y.; Yu, H.-Z.; Fu, Y. *Organometallics* **2013**, *32*, 926−936. (c) Li, Y.; Lin, Z. Y. *J. Org. Chem.* **2013**, *78*, 11357−11365. (d) Yu, S. J.; Liu, S.; Lan, Y.; Wan, B. S.; Li, X. W. *J. Am. Chem. Soc.* **2015**, *137*, 1623−1631. (e) Xu, X. F.; Liu, P.; Shu, X. Z.; Tang, W. P.; Houk, K. N. *J. Am. Chem. Soc.* **2013**, *135*, 9271−9274.
(19) We also computed the alternative C(acyl)−C(sp^3) bond activation of **reactant**. The energy of this transition state (i.e., **L1-TS1a**) is +11.7 kcal/mol, which is 0.6 kcal/mol higher than that of **L1-TS1**. See the Supporting Information for more details.
(20) For similar DFT studies of decarbonylation process, please see: (a) Hong, X.; Liang, Y.; Houk, K. N. *J. Am. Chem. Soc.* **2014**, *136*, 2017−2025. (b) Lu, Q. Q.; Yu, H. Z.; Fu, Y. *J. Am. Chem. Soc.* **2014**, *136*, 8252−8260.
(21) For a recent report about the decarbonylation of the acyl-Rh(III)−H complex, see: Fristrup, P.; Kreis, M.; Palmelund, A.; Norrby, P.; Madsen, R. *J. Am. Chem. Soc.* **2008**, *130*, 5206−5212.
(22) The computational results indicate that Rh−H addition−elimination mechanism is more plausible than the interconversion process from **prod1-c2** and **prod1-c3** in both kinetics and thermodynamics (please see page S4 for more details).
(23) For selected examples of M−H addition−elimination mechanism, see: (a) Xu, L. P.; Hilton, M. J.; Zhang, X. H.; Norrby, P. O.; Wu, Y. D.; Sigman, M. S.; Wiest, O. *J. Am. Chem. Soc.* **2014**, *136*, 1960−1967. (b) Dang, Y. F.; Qu, S. L.; Wang, Z. X.; Wang, X. T. *J. Am. Chem. Soc.* **2014**, *136*, 986−998. (c) Matsuda, T.; Shigeno, M.; Murakami, M. *J. Am. Chem. Soc.* **2007**, *129*, 12086−12087.
(24) The π-allyl mechanism in Rh-catalyzed decarbonylative coupling reaction involves acyl-H reductive elimination, allyl C−H activation, migration insertion, and acyl-H oxidative addition. For energy profiles and concerned discussion of π-allyl mechanism, please see the Supporting Information for more details.
(25) For a recent experimental study on acyl-Rh(III)−H complex which isomerizes the intramolecular alkene, see: Yip, S. Y. Y.; Aissa, C. *Angew. Chem., Int. Ed.* **2015**, *54*, 6870−6873.
(26) Although energy differences among the three competing pathways are small, the computational results are consistent with the fact that these three products were obtained experimentally. Besides, other different computational methods also show similar product distribution with the observed selectivity. Please see the Supporting Information for more details.
(27) For selected examples of similar arm-off mechanisms of the bidentate phosphine ligands, please see: (a) Hamann, B. C.; Hartwig, J. F. *J. Am. Chem. Soc.* **1998**, *120*, 3694−3703. (b) Kawatsura, M.; Hartwig, J. F. *J. Am. Chem. Soc.* **1999**, *121*, 1473−1478. (c) Birkholz, M. N.; Freixa, Z.; van Leeuwen, P. W. *Chem. Soc. Rev.* **2009**, *38*, 1099−1118.
(28) The bidentate alkene insertion transition state **L2-TS2a** is 0.8 kcal/mol higher than **L2-TS2**.
(29) The involvement of solvent molecule (i.e., THF) in the catalytic cycles was also investigated. Because the Rh center of related intermediates and transition states is sterically hindered, the coordination of solvent increases the instability of these intermediates and transition states. Therefore, solvent molecule has no impact on the detailed mechanisms and the selectivity. See page S6 for details.
(30) Marcone, J. E.; Moloy, K. G. *J. Am. Chem. Soc.* **1998**, *120*, 8527−8528.

DOI: 10.1021/acscatal.5b00891
ACS Catal. 2015, 5, 4881−4889